International Journal of Recent Technology and Engineering (IJRTE)
ISSN: 2277-3878 (Online), Volume-12 Issue-3, September 2023

Calibration Considering the Direction of Rotation for Contact Type Three-Dimensional Position-Measuring Instruments

Hirofumi Maeda

Abstract*: In Japan, the aging of sewage facilities due to long-term use has become a significant social issue. As a result, there has been a growing interest in portable and easy-to-operate standalone pipe inspection robots in recent years. However, the pipes being inspected not only have level differences due to joint connections but also pose a high risk of toppling over due to deterioration, collapses, and sludge caused by external disturbances. Many standalone robots address this by suppressing tipping through tire shape and axle adjustments. However, this method is for suppression and not complete prevention. Therefore, we are exploring a software-based approach to prevent tipping through control of robot movement and aiming to achieve advanced self-position estimation. Currently, we are in the stage of verifying this self-position estimation. However, due to the curved nature of the pipes, it is difficult to accurately measure the robot's position and orientation using conventional measurement instruments. Thus, we have developed a specialized three-dimensional position measurement instrument for pipe inspection robots. Furthermore, although we performed calibration in the translational direction of the instrument, while improvements in accuracy were observed in the translational direction, the accuracy in the rotational direction deteriorated. In this paper, we propose a method to simultaneously calibrate the translational and rotational accuracy of the instrument to address this issue. We discuss the mechanism model, calibration parameters, elimination of redundant parameters by introducing redundancy, and parameter estimation using the Newton method. Additionally, through comparative validation using the instrument, we confirm that the position accuracy after calibration is within the range of approximately ±1.0 mm, and the orientation accuracy is within the range of approximately ±0.3 degrees. This demonstrates the effectiveness of the proposed method.

***Keywords*: Measuring Instrument, Calibration, Contact Type, Exploration Robot, Water Pipe**

I. INTRODUCTION

In Japan, the aging of sewage facilities due to long-term use has become a significant social problem. Particularly for facilities that have exceeded the standard service life of 50 years for sewer pipes, there is a high risk of road collapses at any moment. As a result, sampling inspections of pipelines are now being expanded to comprehensive inspections, and inspections using robots have been introduced to alleviate the burden on workers [1]. Many robots used in pipe inspections are operated remotely from within a vehicle called a transport vehicle, which is positioned on the ground. With this approach, the self-propelled robot itself only needs to have essential functions, allowing for lightweight construction and improved maneuverability. Moreover, control and monitoring are performed through remote operation by an operator, enabling immediate response to unforeseen situations. On the other hand, there are challenges associated with securing the location for the transport vehicle and implementing traffic regulations at the worksite. These factors not only increase costs but also impose a significant burden on the operator.

Therefore, there has been a growing interest in portable and easy-to-operate standalone pipe inspection robots in recent years. However, standalone robots have not been widely adopted, and there is a limited variety available. Particularly in Japan, where pipes with a diameter of 150 mm are commonly used, many of the robots used overseas, which are designed for pipes with a diameter of 200 mm or more, do not support the 150 mm diameter [2],[3],[4]. Against this backdrop, we have been conducting research and development to realize a small, portable, and autonomous pipe inspection robot. Our goal is to make it practical and usable in the field [5],[6],[7],[8],[9].

To realize an autonomous robot, it is essential that the robot itself does not topple over inside the pipes. However, the pipes being inspected pose a high risk of tipping over due to various external disturbances, including level differences caused by joint connections and the presence of collapses and sludge due to aging. While preventing tipping over is relatively straightforward in a wired remote-control system where an operator is constantly controlling and monitoring the robot, standalone robots, including our own, must ensure their own stability without external control, and all the necessary features must be incorporated into a small robot body. Many standalone robots, including ours, employ techniques such as adjusting tire shape and axle positions to suppress tipping over. However, these methods are for suppression and not complete prevention. Therefore, we are exploring a software-based approach that focuses on control during movement to prevent tipping over, and we aim to achieve advanced self-position estimation, which is necessary for implementing this strategy [10,11].

Manuscript received on 13 July 2023 | Revised Manuscript received on 18 July 2023 | Manuscript Accepted on 15 September 2023 | Manuscript published on 30 September 2023.
*****Correspondence Author(s)
Hirofumi Maeda*, Department of Information Science and Technology, National Institute of Technology (KOSEN), Yuge College, Ehime Prefecture, Japan. Email: maeda@info.yuge.ac.jp, ORCID ID: 0000-0002-7145-3889.

Currently, we are in the stage of validating this self-localization method. However, due to the curved nature of the pipes, it is challenging to accurately measure the position and orientation of the robot using conventional measurement instruments. Therefore, we have developed a specialized 3D position measurement instrument specifically for pipe inspection robots [12,13,14,15,16,17,18]. This measurement instrument employs a contact-based approach to achieve high accuracy, but it has a higher number of components and a more complex structure compared to non-contact methods. As a result, assembly errors, machining errors, encoder offsets, and other factors introduce cumulative errors that result in significant inaccuracies in the position and orientation of the measurement instrument's tip, which serves as the measurement point. To address this issue, we performed calibration in the translational direction of the instrument. Although improvements in accuracy were observed in the translational direction, there was a decrease in accuracy in the rotational direction [19].

In this paper, we propose a method to simultaneously calibrate the translational and rotational accuracy of the measurement instrument to address this issue. By calibrating both directions together, we aim to improve the overall accuracy of the instrument. Additionally, we conduct comparative validation between the measurements taken before and after calibration to assess the effectiveness of the calibration process.

II. THE CONTACT TYPE THREE-DIMENSIONAL POSITION-MEASURING INSTRUMENT

As shown in Figure 1, the contact-based 3D position measurement instrument is installed in a suspended position directly above the pipe. It is mounted in a way that allows it to hover just above the surface of the pipe.

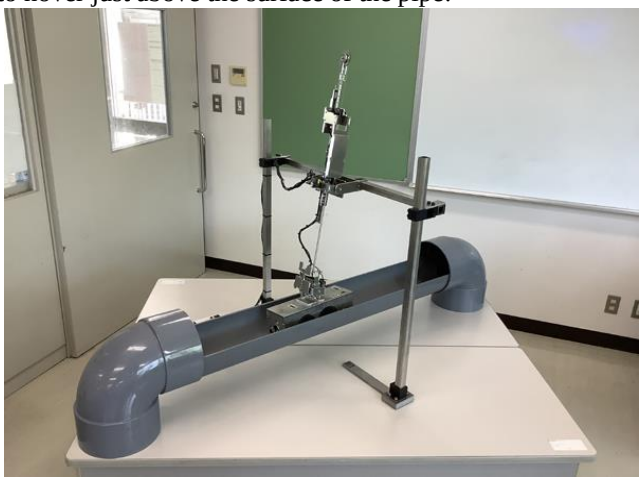

Fig. 1. Installation of the Contact Type Three-Dimensional Position-Measuring Instrument

Figure 2 shows the contact-type three-dimensional position-measuring device used in this study. In addition, a 6-axis stage for accuracy validation is installed directly below the measuring instrument as shown in Figure 3. This measuring instrument consists of 6 degrees of freedom, and an encoder is attached to each joint as shown in Figure 4. This measuring instrument consists of 6 degrees of freedom in Figure 4, and encoders are attached to each joint. A wire is used for J_3, and rotary encoders are used for J_1, J_2, and J_4 to J_6.

Fig. 2. The Contact Type Three-Dimensional Position-Measuring Instrument and the 6-Axis Stage

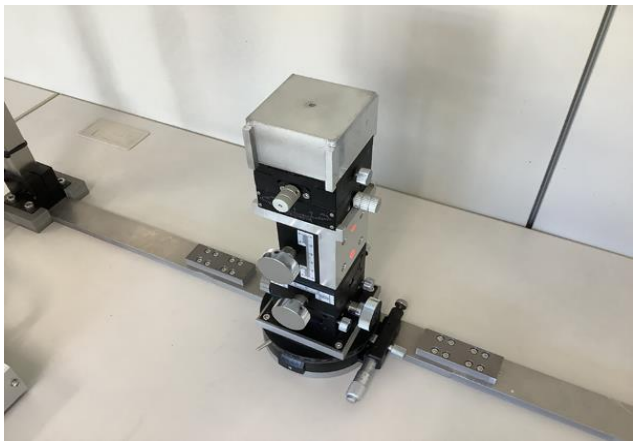

Fig. 3. The 6-Axis Stage for Accuracy Verification

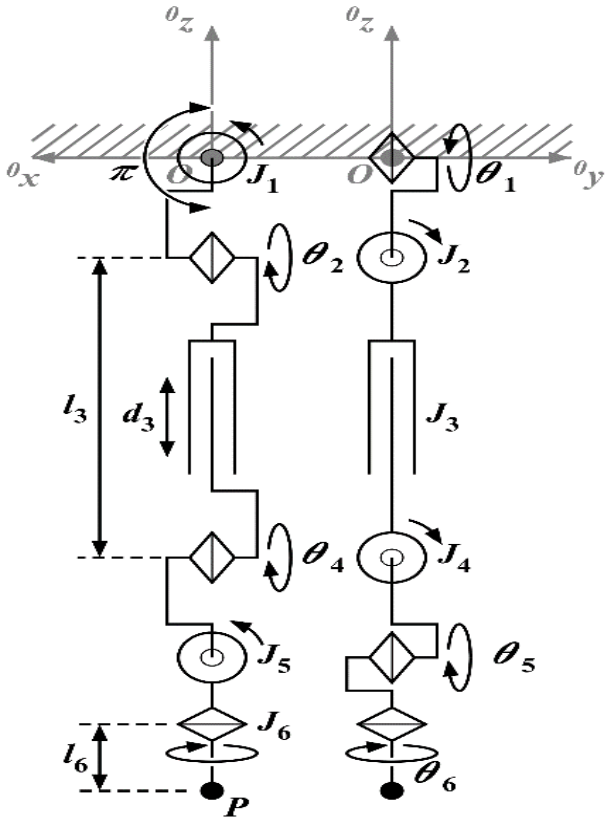

Retrieval Number: 100.1/ijrte.C78670912323
DOI: 10.35940/ijrte.C7867.0912323
Journal Website: www.ijrte.org

Published By:
Blue Eyes Intelligence Engineering
and Sciences Publication (BEIESP)

J_1-J_6 : the position of each joint
P : the position of the end effector
θ_1, θ_2, θ_4- θ_6 : θ_1 to θ_6 excluding θ_3 each indicates the rotation angles for J_1 to J_6 excluding J_3 [rad]
d_3 : d_3 indicates the displacement for J_3 [m]
l_3 : l_3 indicates the initial link length for J_3 [m]
l_6 : link length of the end effector [m]
※ The joint pair of J_1 and J_2 shares the same axis, so do the another joint pair of J_4, J_5 and J_6, which leads to there is no link length between each joint pair.

Fig. 4 Link Structure of the Contact Type Three-Dimensional Position-Measuring Instrument

A significant feature of this measurement instrument is that it is suspended right above during operation. Normally, when the pipe inspection robot is connected to the instrument through its attachment point, it is subject to two disturbances: "the weight of the instrument on the robot" and "the inertia moment around the attachment point between the instrument and the robot." However, if these disturbances can be reduced to a level significantly smaller than the torque generated by the robot, they will have minimal impact on the robot's movement.

To achieve this, as shown in Figure 5, a pulley is attached to the second link. By hanging a weight equivalent to the mass of the instrument from the pulley via a wire, "the weight of the instrument on the robot" is virtually reduced to zero. Specifically, all the weight is constantly supported by the mounting frame of the instrument, eliminating the load on the pipe inspection robot. Next, by aligning the rotation axes of each joint with the center of gravity axis of the object, the inertia moment around the attachment point between the instrument and the robot is minimized. As a result, only the inertia moments of each joint when rotating around the axis passing through the center of gravity of the object remain as disturbances on the robot. Consequently, "the inertia moment around the attachment point between the instrument and the robot" is minimized. Combining this with the lightweight nature of the instrument, disturbances can be suppressed to a negligible level.

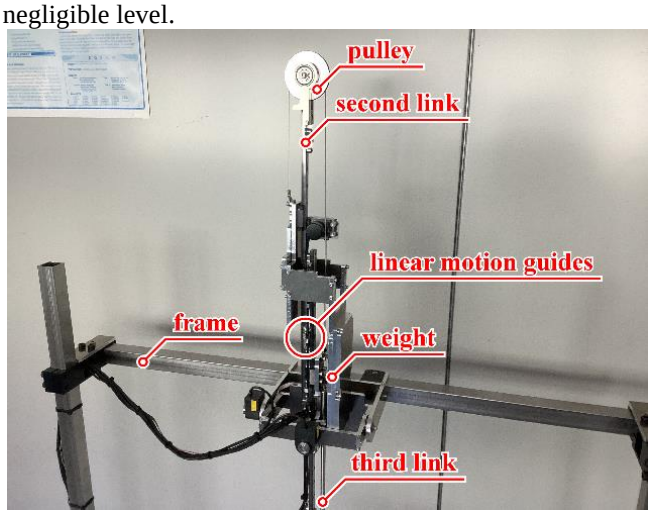

Fig. 5. The Mounting Part and the Pulley Part of the Contact Type Three-Dimensional Position-Measuring Instrument

The position and orientation of the robot attached to the tip of the measurement instrument are calculated based on the sensor values from encoders attached to each joint of the instrument (Figure 6). The encoders used are the UN-2000 and DX-025 from MUTOH INDUSTRIES CO., LTD. They are connected to the STK-7125, manufactured by Alpha Project Co., Ltd., which is installed inside the control circuitry (Figure 7) using open collectors. The STK-7125 utilizes the phase counting mode to calculate the rotation angle from the difference between the A and B phases. Subsequently, the encoder values obtained from the STK-7125 are transmitted to an iPad via BLE. Finally, on the iPad, the joint angles are derived and integrated from the encoder values. Using this data, the position and orientation of the robot are calculated.

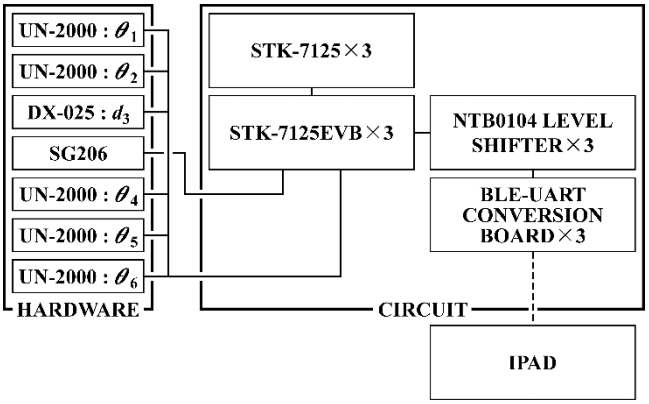

Fig. 6. Schematic Diagram of the System

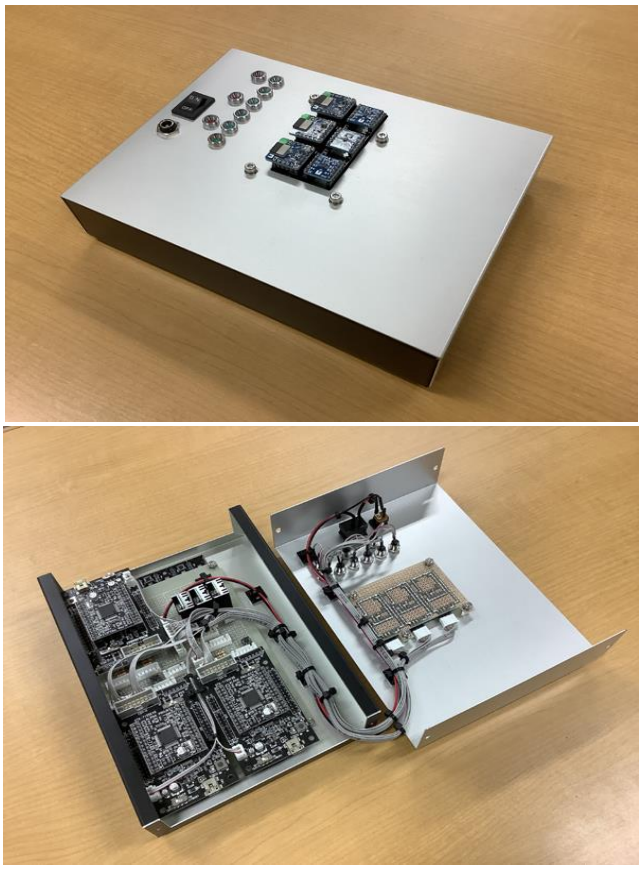

Fig. 7. The Control Circuit of the Measuring Instrument

Published By:
Blue Eyes Intelligence Engineering and Sciences Publication (BEIESP)

III. CALIBRATION METHOD

In this chapter, we propose a method to simultaneously calibrate the translational and rotational directions based on our previously proposed calibration method for the translational direction in reference 19. In addition, to ensure that the calibrated parameters do not deviate significantly from the actual values, we introduce a range of settings for the calibration parameters. Additionally, we propose a solution to address the issues that may arise due to these limitations and incorporate it into the calibration method.

A. Kinematic Model and Calibration Parameters

In the measurement instrument, a kinematic model and corresponding parameters are established for calibration purposes. The instrument possesses 6 degrees of freedom, with an assigned coordinate system for each. Due to the presence of errors between adjacent coordinate systems, calibration parameters are introduced to account for translation distances and rotation angles. These parameters are associated with position and posture, yielding a set of six parameters for each degree of freedom. Consequently, the kinematic model of this 6-degree-of-freedom measuring instrument is composed of a total of 36 parameters.

Here, θ_1, θ_2, d_3, θ_4 to θ_6 in Fig. 3, and the offset value of each encoder are described. The relationship between the encoder value E_i and the rotation angle θ_i at each joint can be expressed by equation (1), and the relationship between the encoder value E_3 and displacement d_3 at joint J_3 is expressed by equation (2).

$$E_i = C_i \cdot \theta_i + O_i \quad (i = 1, 2, 4, 5, 6) \tag{1}$$

$$E_3 = C_3 \cdot d_3 + O_3 \tag{2}$$

where C_i are the known constants of proportionality and O_i are the offset values of the encoders. Also, if E_i (i = 1 to 6) can be detected, O_i can be converted to the target parameter for calibration.

B. Setting Calibration Parameters

The kinematic models based on vector notation exhibit functional duplication in translation and rotation across coordinate systems, resulting in redundant parameters. Thus, it becomes crucial to eliminate unnecessary parameters that contribute to this redundancy.

First, a point P_a is placed at the tip of the measuring instrument as a measurement reference point for calibration. Next, if $\boldsymbol{q}$ is a vector whose elements are n unknown parameters, the relationship between vector $\boldsymbol{p}$ (6×1) representing the position of reference point P_a and vector $\boldsymbol{q}$ can be expressed by equation (3). This $\boldsymbol{p}$ represents only the position (3 × 1) in the previously proposed method. But in this method, the calibration in the translational and rotational directions can be performed simultaneously due to adding three elements representing the posture.

$$\boldsymbol{p} = f(\boldsymbol{q}) \tag{3}$$

In addition, taking $\Delta\boldsymbol{p}$ for the deviation between the measured value of the reference point P_a based on the parameters of the kinematic model and its actual value, it is approximated by the sum of linear combinations of small fluctuations of each parameter. Therefore, it can be expressed by equation (4).

$$\Delta\boldsymbol{p} = (\partial\boldsymbol{p}/\partial\boldsymbol{q}) \cdot \Delta\boldsymbol{q} = A \cdot \Delta\boldsymbol{q} \tag{4}$$

where A is the Jacobian matrix ($6\times n$) concerning the parameters. Furthermore, the corresponding vector $\boldsymbol{r}$ ($6m \times 1$) and extended Jacobian matrix B ($6m \times n$) are obtained if position data for m points P_a are done, so equation (5) holds.

$$\Delta\boldsymbol{r} = B \cdot \Delta\boldsymbol{q} \tag{5}$$

Also, $\Delta\boldsymbol{r}$ and B are $\Delta\boldsymbol{r} = \left[\Delta\boldsymbol{p}_1^T \quad \Delta\boldsymbol{p}_2^T \quad \cdots \quad \Delta\boldsymbol{p}_m^T\right]^T$ and $B = [A_1^T \quad A_2^T \quad \cdots \quad A_m^T]^T$, respectively. Measurements more than 1/6 of n are required for the inverse transform of B to exist, which can reduce the number of it to half that of the previously proposed method.

Here, B is constructed by substituting the measured value of the reference point P_a at different positions and postures of the measuring instrument, the offset value of the encoder, and the initial values of each parameter into the obtained equation (5). Next, the gap between each value becomes large since the elements of B include length, angle, etc. Therefore, they are normalized using appropriate numerical values. In this study, we used the square root of the sum of squares of the elements in each column of B as an appropriate numerical value.

Next, obtain the pseudo-inverse matrix of the normalized matrix B. Since a general pseudo-inverse matrix may diverge, the singular value decomposition method is used to find it. The singular value decomposition of matrix B obtains equations (6) and (7).

$$B = U \cdot S \cdot V^T \tag{6}$$

$$S = \begin{array}{c} \\ \end{array}\begin{array}{c} \begin{array}{cc} h & n-h \end{array} \\ \begin{bmatrix} G_{11} & 0 \\ 0 & 0 \end{bmatrix} \end{array} \qquad G_{11} = \mathrm{diag}(\sigma_1 \quad \sigma_2 \quad \cdots \quad \sigma_h) \tag{7}$$

Since both U and V are orthogonal matrices, which are $6m \times 6m$ and $n \times n$ matrices, respectively. Therefore, the pseudo-inverse of the normalized matrix B is obtained from equation (6). From this result, the rank of B corresponds to that of G_{11} can be obtained. The rank of B is less than all parameter numbers set in the instrument. Therefore, the number of parameters can be reduced to rank by selectively removing redundant them. To reduce the number of parameters, equation (7) is focused. First, the orthogonal matrices U and V are decomposed into two by the rank h since h is the rank of B, and let $U = [U_1 \quad U_2]$ and $V = [V_1 \quad V_2]$. V2 corresponds to a singular value of 0, and the parameters whose absolute values of the elements in each column of V_2 are close to 1.0 are candidates for deletion. Also, elements in this sequence with the same absolute value but different signs mean that the parameters corresponding to those elements overlap each other.

The redundant parameters that overlap with important parameters such as encoder offset values and link lengths are prioritized for elimination. However, if it is more convenient for calculations and control to remove important parameters, they may not be eliminated.

Retrieval Number: 100.1/ijrte.C78670912323
DOI: 10.35940/ijrte.C7867.0912323
Journal Website: www.ijrte.org

Published By:
Blue Eyes Intelligence Engineering
and Sciences Publication (BEIESP)

Additionally, when two redundant parameters correspond to rotation angles or displacements, one of them is removed. In the case of the measurement instrument's absolute coordinate system, one of the coordinate axes of a particular coordinate system and the rotation axis of the first link, which corresponds to the encoder's offset value, will always overlap. Furthermore, among the translational parameters representing the error between the instrument's end effector P and the reference point P_a, one of them will always become a redundant parameter and needs to be excluded. It is acceptable to remove this redundant parameter from the mechanism model at an early stage without causing any issues.

This process describes the steps for removing unnecessary redundant parameters and reconstructing the mechanism model accordingly. Additionally, the estimation algorithm using the Newton method, which will be described next, is used to determine the true values of the calibration parameters. As mentioned earlier, this method employs a range of settings for the calibration parameter values, so the Newton method is performed in two stages with different conditions.

C. First Parameter Estimation by Newton's Method

As in Section B, B is constructed by substituting the measured value of the reference point P_a at different positions and postures of the measuring instrument, the offset value of the encoder, and the initial values of each parameter into equation (5). Next, the pseudo-inverse matrix of B is obtained using equation (6) without normalization, unlike Section B.

Here, equation (6) is replaced with equation (8) using U_1 and V_1.

$$B = U_1 \cdot G_{11} \cdot V_1^T \tag{8}$$

Furthermore, by transforming equation (8), the pseudo-inverse matrix B^+ is expressed by equation (9).

$$\begin{aligned} B^+ &= V_1 \cdot G_{11}^{-1} \cdot U_1^T \\ G_{11} &= \mathrm{diag}(1/\sigma_1 \quad 1/\sigma_2 \quad \dots \quad 1/\sigma_h) \end{aligned} \tag{9}$$

Therefore, the relationship of equation (11) finds between $\boldsymbol{q}_i$ before modification and $\boldsymbol{q}_{i+1}$ after modification because formula (5) is transformed into formula (10).

$$\Delta \boldsymbol{q} = B^+ \cdot \Delta \boldsymbol{r} \tag{10}$$

$$\boldsymbol{q}_{i+1} = \boldsymbol{q}_i + \Delta \boldsymbol{q} \tag{11}$$

The true values of n calibration parameters $\boldsymbol{q}$ are estimated by substituting this modified $\boldsymbol{q}_{i+1}$ into Equation (5) and repeating the calculation until $\Delta \boldsymbol{q}$ converges approximately 0.

However, in practice, the calibration parameter values do not converge with this method for two reasons. The first reason is that, as in the previously proposed method, the latter elements of G_{11} approach 0 infinitely but do not completely do, so the latter elements of reciprocal G_{11}^{-1} are large numbers. The second reason is that by setting a range for the calibration parameter values so that the values do not differ greatly from the actual, the fluctuation range of the calibration parameter values is small, and $\Delta \boldsymbol{q}$ is larger than the range. Therefore, the problem is solved in the latter elements of G_{11}^{-1} are set to 0 using a using low-rank approximation like last time. Specifically, to prevent the calibration parameter values from oscillating, the elements of G_{11}^{-1} are to leave the original values as much as possible so that the two correlated calibration parameters do not overshoot the minimum and maximum values of the setting range. However, unlike the previous time, most of the elements of G_{11}^{-1} are set to 0 using a low-rank approximation to suppress the amount of change in $\Delta \boldsymbol{q}$, resulting in insufficient calibration. Therefore, setting the following new conditions and performing the second parameter estimation by Newton's method.

D. Second Parameter Estimation by Newton's Method

Perform a second Newton's method, including the elements of G_{11}^{-1} that are zeroed using the low-rank approximation of Section C. However, if the elements of G_{11}^{-1} are used as they are, the value of $\Delta \boldsymbol{q}$ corresponding to the correction value becomes too large, and the calibration parameter value oscillates and does not converge.

Therefore, by replacing the elements of G_{11}^{-1} that are set to 0 using the low-rank approximation to small values of 1 or less and performing Newton's method, the oscillation of the calibration parameters is suppressed. As a result, although the number of times until convergence increases, calibration can be performed reliably. However, even in this case, if the number of times is repeated, the calibration parameter value swings off to the minimum or maximum value. Therefore, the ideal calibration parameter values are obtained by finishing the calibration before the calibration parameter values swing out of the range. Finally, the mean error of $\boldsymbol{r}$ is subtracted from the estimate to remove the installation error caused by the calibration parameter converging near the maximum or minimum value of the set range.

IV. ACCURACY VERIFICATION

As in III, part of the paragraph on reference 19 is quoted for comparison with them. In the contact type three-dimensional position-measuring instrument shown in Fig. 4, six-coordinate systems are set for the directions of the orthogonal rotation axes of each joint. Let the position of $[x_{p0} \quad y_{p0} \quad z_{p0}]$ from the origin P_0 of the absolute coordinate system be the coordinate system P_1 of J_1, and use these three elements as parameters. Next, since the rotation axis is around the y-axis in the torsion angle at P_1, as described in A of III, the parameter is set to $[\alpha_1 \quad O_1 \quad \gamma_1]$ by replacing the offset value of the encoder with a parameter. Similarly, set the coordinate systems P_2 to P_6 of J_2 to J_6, and set the respective parameters to $[x_{p1} \quad y_{p1} \quad z_{p1}]$, $[O_2 \quad \beta_2 \quad \gamma_2]$, $[x_{p2} \quad y_{p2} \quad z_{p2}]$, $[\alpha_3 \quad \beta_3 \quad \gamma_3]$, $[x_{p3} \quad y_{p3} \quad l_3 + O_3]$, $[O_4 \quad \beta_4 \quad \gamma_4]$, $[x_{p4} \quad y_{p4} \quad z_{p4}]$, $[\alpha_5 \quad O_5 \quad \gamma_5]$, $[x_{p5} \quad y_{p5} \quad z_{p5}]$, $[\alpha_6 \quad \beta_6 \quad O_6]$, $[0 \quad 0 \quad l_6]$, so there are 38 initial parameters in total. Table 1 shows the initial values of the parameters and the proportionality constants of C_1 to C_6.

Published By:
Blue Eyes Intelligence Engineering
and Sciences Publication (BEIESP)

Table 1. Initial Parameters and Constant of Proportionality

x_{p0} [m]	y_{p0} [m]	z_{p0} [m]	α_1 [rad]	O_1 [ ]	γ_1 [rad]
0	0	0	0	-3682	0

x_{p1} [m]	y_{p1} [m]	z_{p1} [m]	O_2 [ ]	β_2 [rad]	γ_2 [rad]
0	0	0	676	0	0

x_{p2} [m]	y_{p2} [m]	z_{p2} [m]	α_3 [rad]	β_3 [rad]	γ_3 [rad]
0	0	0	0	0	0

x_{p3} [m]	y_{p3} [m]	l_3 [m]	O_3 [ ]	O_4 [ ]	β_4 [rad]
0	0	0.145	-25165	617	0

γ_4 [rad]	x_{p4} [m]	y_{p4} [m]	z_{p4} [m]	α_5 [rad]	O_5 [ ]
0	0	0	0	0	281

γ_5 [rad]	x_{p5} [m]	y_{p5} [m]	z_{p5} [m]	α_6 [rad]	β_6 [rad]
0	0	0	0	0	0

O_6 [ ]	l_6 [m]
-1886	0.0425

C_1 [ ]	C_2 [ ]	C_3 [ ]	C_4 [ ]	C_5 [ ]	C_6 [ ]
1273.24	1273.24	100000.00	-1273.24	1273.24	1273.24

Next, the reference point P_a [x_{pa} y_{pa} z_{pa} α_{pa} β_{pa} γ_{pa}]was measured at 12 points in combinations of x_{pa} = -20.0, 20.0 mm, y_{pa} = -20.0, 20.0 mm, z_{pa} = -373.0, -363.0, -353.0 mm, and $\alpha_{pa} = \beta_{pa} = \gamma_{pa}$ = 0.0 degrees to set the calibration parameters. Table 2 shows the measurement results. The resolutions of the encoders used at quadruple multiplication are 0.045 degrees to the rotation direction at the UN-2000 and 0.01 mm to the translation direction at the DX-025. All of them are used in quadruple multiplication.

Table 2. Measurement Data for Setting Calibration Parameters

reference point						measured value					
x_{pa} [m]	y_{pa} [m]	z_{pa} [m]	α_{pa} [deg]	β_{pa} [deg]	γ_{pa} [deg]	x_{pa} [m]	y_{pa} [m]	z_{pa} [m]	α_{pa} [deg]	β_{pa} [deg]	γ_{pa} [deg]
-0.020	-0.020	-0.373	0.000	0.000	0.000	-0.02011	-0.01884	-0.37299	0.23	0.13	0.35
-0.020	-0.020	-0.363	0.000	0.000	0.000	-0.02027	-0.01874	-0.36303	0.27	0.13	0.21
-0.020	-0.020	-0.353	0.000	0.000	0.000	-0.02010	-0.01861	-0.35308	0.31	0.09	0.30
0.020	-0.020	-0.373	0.000	0.000	0.000	0.01955	-0.01962	-0.37295	359.87	0.27	0.31
0.020	-0.020	-0.363	0.000	0.000	0.000	0.01971	-0.01951	-0.36303	359.91	0.27	0.49
0.020	-0.020	-0.353	0.000	0.000	0.000	0.01958	-0.01912	-0.35301	359.96	0.27	0.31
-0.020	0.020	-0.373	0.000	0.000	0.000	-0.02001	0.02034	-0.37301	0.04	0.00	359.14
-0.020	0.020	-0.363	0.000	0.000	0.000	-0.02017	0.02078	-0.36306	0.09	0.00	359.18
-0.020	0.020	-0.353	0.000	0.000	0.000	-0.02030	0.02038	-0.35303	0.09	0.00	359.32
0.020	0.020	-0.373	0.000	0.000	0.000	0.01962	0.02018	-0.37301	359.82	0.18	0.26
0.020	0.020	-0.363	0.000	0.000	0.000	0.01953	0.02011	-0.36305	359.87	0.18	0.26
0.020	0.020	-0.353	0.000	0.000	0.000	0.01965	0.01969	-0.35304	359.82	0.18	359.72

Based on the data in Table 2, unnecessary redundant parameters have been deleted using method B in III. The rank of B becomes 25, and redundant parameters were deleted from the condition of B in III for the elements for each column of V_2.

Next, the calibration parameters have been estimated by the first Newton's method shown in C of III. Table 3 shows the initial values of 25 calibration parameters and estimated results based on the state of convergence. Since O_2 and z_{p3} among the parameters deleted from the 38 initial parameters in Table 1 had initial values , they were replaced with the initial values of the duplicated calibration parameters α_1 and O_3, respectively. This hastened the convergence of Newton's method and reduced the number of estimations.

Finally, the parameters were estimated by the second Newton method shown in D of III using the parameter value of $\boldsymbol{q}_5$ in Table 3. In the first Newton's method, the value that became 0 by the low-rank approximation was replaced with 0.1 in the second Newton's method. As a result, the calibration parameters converged values in Table 4. In addition, the calculation is performed using this calibration parameter when estimating, and the position and posture are obtained by subtracting the average error of $\boldsymbol{r}$ from the estimation result.

Table 3. First Calibration Parameters

	$\boldsymbol{q}_0$	$\boldsymbol{q}_1$	$\boldsymbol{q}_2$	$\boldsymbol{q}_3$	$\boldsymbol{q}_4$	$\boldsymbol{q}_5$
x_{p0} [mm]	0.00000	-0.00004	-0.00004	-0.00004	-0.00004	-0.00004
y_{p0} [mm]	0.00000	-0.00016	-0.00018	-0.00018	-0.00018	-0.00018
z_{p0} [mm]	0.00000	-0.00001	-0.00019	-0.00019	-0.00019	-0.00019
α_1 [rad]	-0.53093	-0.53073	-0.53073	-0.53073	-0.53073	-0.53073
O_1 [ ]	-3682.00000	-3682.00000	-3682.00000	-3682.00000	-3682.00000	-3682.00000
γ_1 [rad]	0.00000	-0.00005	-0.00005	-0.00005	-0.00005	-0.00005
z_{p1} [mm]	0.00000	-0.00007	0.00007	0.00007	0.00007	0.00007
γ_2 [rad]	0.00000	-0.00031	-0.00031	-0.00031	-0.00031	-0.00031
β_3 [rad]	0.00000	-0.00069	-0.00069	-0.00069	-0.00069	-0.00069
y_{p3} [mm]	0.00000	-0.00016	-0.00018	-0.00018	-0.00018	-0.00018
O_3 [ ]	-39665.00000	-39598.33333	-39598.33333	-39598.33333	-39598.33333	-39598.33333
O_4 [ ]	617.00000	617.00000	617.00000	617.00000	617.00000	617.00000
β_4 [rad]	0.00000	-0.00070	-0.00070	-0.00070	-0.00070	-0.00070
γ_4 [rad]	0.00000	0.00005	0.00005	0.00005	0.00005	0.00005
x_{p4} [mm]	0.00000	0.00003	0.00004	0.00004	0.00004	0.00004
z_{p4} [mm]	0.00000	0.00001	0.00019	0.00019	0.00019	0.00019
α_5 [rad]	0.00000	0.00014	0.00014	0.00014	0.00014	0.00014
O_5 [ ]	281.00000	281.00000	281.00000	281.00000	281.00000	281.00000
γ_5 [rad]	0.00000	0.00005	0.00005	0.00005	0.00005	0.00005
x_{p5} [mm]	0.00000	0.00004	0.00003	0.00003	0.00003	0.00003
y_{p5} [mm]	0.00000	-0.00016	-0.00018	-0.00018	-0.00018	-0.00018
α_6 [rad]	0.00000	0.00014	0.00014	0.00014	0.00014	0.00014
β_6 [rad]	0.00000	-0.00070	-0.00070	-0.00070	-0.00070	-0.00070
O_6 [ ]	-1886.00000	-1886.00000	-1886.00000	-1886.00000	-1886.00000	-1886.00000
d_6 [mm]	0.04250	0.04251	0.04269	0.04269	0.04269	0.04269

Published By:
Blue Eyes Intelligence Engineering
and Sciences Publication (BEIESP)

Table 4. Second Calibration Parameters

	q_0	q_1	q_2	q_{10}	q_{11}	q_{12}
x_{p0} [mm]	-0.00004	0.00001	-0.00001	-0.00104	-0.00118	-0.00133
y_{p0} [mm]	-0.00018	-0.00025	-0.00029	-0.00013	-0.00006	0.00003
z_{p0} [mm]	-0.00019	0.00007	0.00032	0.00207	0.00226	0.00244
α_1 [rad]	-0.53073	-0.52958	-0.52844	-0.52012	-0.51916	-0.51822
O_1 [ ]	-3682.00000	-3682.00038	-3682.00077	-3682.00382	-3682.00416	-3682.00450
γ_1 [rad]	-0.00005	0.00059	0.00121	0.00580	0.00633	0.00684
z_{p1} [mm]	0.00007	0.00032	0.00055	0.00209	0.00225	0.00240
γ_2 [rad]	-0.00031	-0.00063	-0.00093	-0.00299	-0.00320	-0.00340
β_3 [rad]	-0.00069	0.00008	0.00083	0.00635	0.00697	0.00759
y_{p3} [mm]	-0.00018	0.00006	0.00031	0.00218	0.00240	0.00263
O_3 [ ]	-39598.33333	-39598.33333	-39598.33333	-39598.33333	-39598.33333	-39598.33333
O_4 [ ]	617.00000	617.00020	617.00040	617.00207	617.00229	617.00250
β_4 [rad]	-0.00070	0.00026	0.00120	0.00824	0.00906	0.00986
γ_4 [rad]	0.00005	0.00054	0.00102	0.00428	0.00462	0.00495
x_{p4} [mm]	0.00004	-0.00008	-0.00020	-0.00114	-0.00125	-0.00136
z_{p4} [mm]	0.00019	0.00004	-0.00010	-0.00105	-0.00114	-0.00123
α_5 [rad]	0.00014	-0.00075	-0.00162	-0.00823	-0.00900	-0.00977
O_5 [ ]	281.00000	281.00092	281.00185	281.00927	281.01015	281.01101
γ_5 [rad]	0.00005	0.00046	0.00087	0.00388	0.00422	0.00456
x_{p5} [mm]	0.00003	0.00001	-0.00009	-0.00161	-0.00182	-0.00201
y_{p5} [mm]	-0.00018	-0.00013	-0.00008	-0.00020	-0.00026	-0.00034
α_6 [rad]	0.00014	-0.00012	-0.00038	-0.00218	-0.00237	-0.00256
β_6 [rad]	-0.00070	-0.00227	-0.00382	-0.01528	-0.01661	-0.01791
O_6 [ ]	-1886.00000	-1885.99972	-1885.99943	-1885.99779	-1885.99760	-1885.99740
d_6 [mm]	0.04269	0.04290	0.04309	0.04440	0.04454	0.04467

The accuracy improvement was verified using the calibration parameters obtained in Table 4. P was used as a measurement point different from the reference point P_a used in setting the calibration parameters for accuracy verification. The measurement points P $[x_p \quad y_p \quad z_p \quad \alpha_p \quad \beta_p \quad \gamma_p]$ were set to a combination of x_p = -20.0, 20.0 mm, y_p = -15.0, 15.0 mm, z_p = -373.0, -353.0 mm, $\alpha_p = \beta_p = \gamma_p$ = 0.0 degrees, and measurements were performed with and without calibration. Table 5 shows the measurement results. The accuracy error range required for this instrument is ±1.0 mm for position and ±1.0 deg for posture. In the results of Table 5, the accuracies of the positions x_p, y_p, and z_p are generally within the range of ±1.0 mm, and the accuracies of the attitudes α_p, β_p, and γ_p are within the range of ±0.3 deg after calibration. In addition, the variations corresponding to the standard deviations are generally smaller than before the calibration, demonstrating the effect of the calibration. Some data slightly exceed 1 mm for y_p, but it is considered to be largely due to the error of the 6-axis stage. However, the calibration method presented this time is effective for this measuring instrument since sufficient correction was observed.

Table 5. Verification Results of the Calibration

without calibration																						
reference point							measured value						error									
x_p [m]	y_p [m]	z_p [m]	α_p [deg]	β_p [deg]	γ_p [deg]	x_p [m]	y_p [m]	z_p [m]	α_p [deg]	β_p [deg]	γ_p [deg]	x_p [m]	y_p [m]	z_p [m]	α_p [deg]	β_p [deg]	γ_p [deg]					
-0.020	-0.015	-0.373	0.000	0.000	0.000	-0.02034	-0.01454	-0.37303	-0.04371	0.09059	-0.76769	-0.00034	0.00046	-0.00003	-0.04371	0.09059	-0.76769					
-0.020	-0.015	-0.353	0.000	0.000	0.000	-0.02037	-0.01437	-0.35306	-0.08843	0.13591	-0.59065	-0.00037	0.00063	-0.00006	-0.08843	0.13591	-0.59065					
0.020	-0.015	-0.373	0.000	0.000	0.000	0.01870	-0.01529	-0.37303	0.27322	0.35719	-0.60217	-0.00130	-0.00029	-0.00003	0.27322	0.35719	-0.60217					
0.020	-0.015	-0.353	0.000	0.000	0.000	0.01848	-0.01502	-0.35314	0.13829	0.44892	-0.45923	-0.00152	-0.00002	-0.00014	0.13829	0.44892	-0.45923					
0.020	0.015	-0.373	0.000	0.000	0.000	0.01959	0.01412	-0.37309	0.27145	0.22262	-0.51216	-0.00041	-0.00088	-0.00009	0.27145	0.22262	-0.51216					
0.020	0.015	-0.353	0.000	0.000	0.000	0.01876	0.01374	-0.35319	0.27267	0.40283	-0.46844	-0.00124	-0.00126	-0.00019	0.27267	0.40283	-0.46844					
-0.020	0.015	-0.373	0.000	0.000	0.000	-0.02005	0.01506	-0.37308	0.04523	0.04468	-0.40232	-0.00005	0.00006	-0.00008	0.04523	0.04468	-0.40232					
-0.020	0.015	-0.353	0.000	0.000	0.000	-0.02028	0.01465	-0.35318	0.04490	-0.00028	-0.35707	-0.00028	-0.00035	-0.00018	0.04490	-0.00028	-0.35707					
								average of error				-0.00069	-0.00021	-0.00010	0.11420	0.21281	-0.51997					
								standard deviation of error				0.00053	0.00060	0.00006	0.13751	0.16098	0.12242					

with calibration																						
reference point							measured value						error									
x_p [m]	y_p [m]	z_p [m]	α_p [deg]	β_p [deg]	γ_p [deg]	x_p [m]	y_p [m]	z_p [m]	α_p [deg]	β_p [deg]	γ_p [deg]	x_p [m]	y_p [m]	z_p [m]	α_p [deg]	β_p [deg]	γ_p [deg]					
-0.020	-0.015	-0.373	0.000	0.000	0.000	-0.01997	-0.01542	-0.37289	0.02337	-0.05734	-0.76072	0.00072	-0.00022	0.00021	-0.09083	-0.27015	-0.24076					
-0.020	-0.015	-0.353	0.000	0.000	0.000	-0.01989	-0.01497	-0.35295	-0.02252	-0.01201	-0.58452	0.00080	0.00023	0.00015	-0.13673	-0.22482	-0.06455					
0.020	-0.015	-0.373	0.000	0.000	0.000	0.01909	-0.01585	-0.37297	0.28402	0.20778	-0.68799	-0.00022	-0.00064	0.00013	0.16982	-0.00503	-0.16802					
0.020	-0.015	-0.353	0.000	0.000	0.000	0.01898	-0.01530	-0.35309	0.14506	0.29978	-0.55375	-0.00033	-0.00009	0.00001	0.03086	0.08698	-0.03378					
0.020	0.015	-0.373	0.000	0.000	0.000	0.01966	0.01351	-0.37318	0.28502	0.10162	-0.50275	0.00035	-0.00129	-0.00008	0.17082	-0.11119	0.01721					
0.020	0.015	-0.353	0.000	0.000	0.000	0.01895	0.01340	-0.35328	0.28498	0.28234	-0.46093	-0.00036	-0.00139	-0.00017	0.17078	0.06954	0.05904					
-0.020	0.015	-0.373	0.000	0.000	0.000	-0.02002	0.01414	-0.37309	0.09974	-0.07385	-0.29763	0.00067	-0.00066	0.00001	-0.01447	-0.28666	0.22233					
-0.020	0.015	-0.353	0.000	0.000	0.000	-0.02012	0.01399	-0.35319	0.09995	-0.11821	-0.24624	0.00057	-0.00080	-0.00009	-0.01426	-0.33102	0.27372					
								average of error				0.00027	-0.00061	0.00002	0.03575	-0.13404	0.00815					
								standard deviation of error				0.00047	0.00053	0.00012	0.11471	0.15665	0.16550					

V. CONCLUSION

In this paper, we proposed a method for simultaneously calibrating the translational and rotational accuracies of a contact-type 3D position measurement instrument to address the error issues. We discussed the mechanism model and its calibration parameters, as well as presented a method for removing unnecessary parameters that introduce redundancy. Moreover, we demonstrated the use of a two-stage Newton method to resolve the convergence issue arising from the constraints imposed on the calibration parameter values. In the comparative validation using the measurement instrument, we confirmed that the calibrated positions were generally within a range of approximately ±1.0 mm, and the calibrated orientations were within a range of approximately ±0.3 degrees. The low variability observed in the results highlights the effectiveness of the proposed calibration method for the measurement instrument. Moving forward, we plan to further investigate the following two subjects.

1. **Calibration for the Test Field**
   The calibration performed in this study includes the positional relationship between the measuring instrument, which is an external parameter, and the 6-axis stage. Therefore, estimating the external parameters with the test field is necessary when validating the pipe inspection robot. For that reason, we will establish a method to re-estimate only the external parameters while leaving the internal parameters corresponding to the errors of the measuring instrument itself as they are.
2. **Influence of Tires on Localization**
   In our proposed self-position estimation for pipe inspection robots, we have not considered the impact of tire shape on the deviation of the contact point between the robot and the pipe. Therefore, in future research, we plan to investigate the effects of tire characteristics using the contact-type three-dimensional position measurement instrument developed in this study. By conducting these verifications, we aim to gain a better understanding of the influence of tire shape on the accuracy of self-position estimation in pipe inspection scenarios.

ACKNOWLEDGMENT

This work was supported by Grant-in-Aid for Scientific Research(C) Grant Number 23K04316.

DECLARATION

Funding/ Grants/ Financial Support	Yes, this work was supported by Grant-in-Aid for Scientific Research(C) Grant Number 23K04316.
Conflicts of Interest/ Competing Interests	No conflicts of interest to the best of our knowledge.
Ethical Approval and Consent to Participate	No, the article does not require ethical approval and consent to participate with evidence.
Availability of Data and Material/ Data Access Statement	Not relevant.
Authors Contributions	I am only the sole author of the article.

REFERENCES

1. Japan institute of wastewater engineering technology, “Development foundation survey of sewerage facilities management robot”, Sewer new technology Annual report of the Institute, 1992, pp.43-52.
2. Rome, E., Hertzberg, J., Kirchner, F., Licht, U. and Christaller, T., “Towards Autonomous Sewer Robots: the MAKRO Project”, Urban Water, Vol. 1, 1999, pp. 57-70. [CrossRef]
3. Streich, H. and Adria, O., “Software approach for the autonomous inspection robot MAKRO”, in Proceedings of the 2004 IEEE International Conference Robotics and Automation, 2004, pp. 3411-3416. [CrossRef]
4. Birkenhofer, C., Regenstein, K., Zöllner, J. M. and Dillmann, R., “Architecture of multi-segmented inspection Robot KAIRO-II”, DOI: 10.1007/978-1-84628-974-3_35, In book: Robot Motion and Control, 2007, pp.381-389. [CrossRef]
5. Ayaka, N., Kazutomo, F., Toshikazu, S., Mikio, G. and Hirofumi M., “Prototype design for a piping inspection robot”, 43rd Graduation Research Presentation Lecture of Student Members of the JSME, 2013, 716.
6. Kazutomo, F., Yoshiki, I. and Hirofumi M., “Modularization for a piping inspection robot”, 2013 Symposium on System Integration, 2013, pp.1297-1300.
7. Kazutomo, F., Toshikazu, S., Mikio, G., Yoshiki, I. and Hirofumi M., “Miniaturization of the piping inspection robot by modularization”, 44th Graduation Research Presentation Lecture of Student Members of the JSME, 2014, 613.
8. Hirofumi, M., Takuya, K., Kazutomo, F., Yoshiki, I., Toshikazu, S. and Mikio, G., “Research and development about a piping inspection robot - Report1: Prototype design for a miniaturization -”, Bulletin of National Institute of Technology, Yuge College, Vol. 36, 2014, pp.79-82.
9. Hirofumi, M., Yoshiki, I., Toshikazu, S. and Mikio, G., “Research and development about a piping inspection robot - Report2: Prototype design for maintenance improvement -”, Bulletin of National Institute of Technology, Yuge College, Vol. 37, 2015, pp.75-79.

Published By:
Blue Eyes Intelligence Engineering
and Sciences Publication (BEIESP)

10. Hirofumi M., Ryota, K., “Development of a small autonomous pipe inspection robot (Modularization of hardware using the technique of wooden mosaic work)”, Transactions of the Japan Society of Mechanical Engineers, Vol.82, No.839, 2016, pp.1-16. [CrossRef]
11. Hirofumi M., “Automatic Compensation of the Positional Error Utilizing Localization Method in Pipe”, International Journal of Recent Technology and Engineering (IJRTE), Vol.9, No.6, 2021, pp.151-157. [CrossRef]
12. Yuki, Y., Yoshiki, I., Hirofumi, M., “Self-localization Measurement of the Piping Inspection Robot by a ARtoolkit”, Transactions of the Japan Society of Mechanical Engineers, No. 165-1, 2016, 502.
13. Ayano, T., Hirofumi, M., “Accuracy Improvement of the Measuring Instrument for the Piping Inspection Robot”, The Japan Society of Mechanical Engineers Chugoku-Shikoku Branch, the 47th Conference on the Graduation Thesis for Undergraduate Students,2017, 921.
14. Ayano, T., Hirofumi, M., “Tilt Adjustment to Measuring Instrument for Piping Inspection Robot”, Transactions of the Japan Society of Mechanical Engineers, No. 185-1, 2018, 1304. [CrossRef]
15. Keita I., Hirofumi M., “Hardware Design for the Contact Type Measuring Instrument”, The Japan Society of Mechanical Engineers Chugoku-Shikoku Branch, the 52nd Conference on the Graduation Thesis for Undergraduate Students, 2022, 11b4.
16. Ibuki T., Hirofumi M., “Data Reception of the Contact Type Measuring Instrument using BLE”, Transactions of the Japan Society of Mechanical Engineers, No. 225-1, 2022, 09a1.
17. Kohei S., Hirofumi M., “Posture Measurement of a Robot using the Contact Type Measuring Instrument”, Transactions of the Japan Society of Mechanical Engineers, No. 225-1, 2022, 09a2.
18. Hirofumi M., “A Contact Type Three Dimensional Position Measuring Instrument for Verification of a Piping Inspection Robot”, International Journal of Recent Technology and Engineering (IJRTE), Vol.10, No.6, 2022, pp.65-72.
19. Hirofumi M., “Translational Calibration for Contact Type Three-Dimensional Position-Measuring Instruments”, International Journal of Recent Technology and Engineering (IJRTE), Vol.11, No.5, 2023, pp.9-16. [CrossRef]

AUTHOR PROFILE

Hirofumi Maeda is Professor in the Information Science and Technology Department at National Institute of Technology (KOSEN), Yuge College. Dr. Maeda’s research focuses on the practical application of mechanical engineering, namely, developing rescue robots, pipe inspection robots and natural language processing. Dr. Maeda previously served as a researcher at the NPO International Rescue System Institute. Dr. Maeda is currently a member of the Japan Society of Mechanical Engineers, the Robotics Society of Japan, the Japan Association for College of Technology, and the Japan Institute of Marine Engineering. Dr. Maeda has published 13 peer-reviewed papers and presented 81 papers. In addition, Dr. Maeda received two awards at academic conferences and 15 external funds.